SLAC-PUB-16547

Echo-enabled harmonics up to the 75th order from precisely tailored electron beams

E. Hemsing[1*], M. Dunning[1], B. Garcia[1], C. Hast[1], T. Raubenheimer[1], G. Stupakov[1], and D. Xiang[2,3*]
[1] *SLAC National Accelerator Laboratory, Menlo Park, California 94025, USA*
[2] *Key Laboratory for Laser Plasmas (Ministry of Education), Department of Physics and Astronomy, Shanghai Jiao Tong University, Shanghai 200240, China*
[3] *Collaborative Innovation Center of IFSA (CICIFSA), Shanghai Jiao Tong University, Shanghai 200240, China*
(Dated: April 18, 2016)

The production of coherent radiation at ever-shorter wavelengths has been a long-standing challenge since the invention of lasers[1, 2] and subsequent demonstration of frequency doubling[3]. Modern x-ray free-electron lasers (FELs) use relativistic electrons to produce intense x-ray pulses at few-femtosecond timescales[4–6]. However, the shot noise that seeds the amplification produces pulses with a noisy spectrum and limited temporal coherence. To produce stable transform-limited pulses, a seeding scheme called echo-enabled harmonic generation (EEHG) has been proposed[7, 8] which harnesses the highly nonlinear phase mixing of the celebrated echo phenomenon[9] to generate coherent harmonic density modulations in the electron beam with conventional lasers. Here we report on a demonstration of EEHG up to the 75th harmonic, where 32 nm light is produced from a 2400 nm laser. We also demonstrate that individual harmonic amplitudes are controlled by simple adjustment of the phase mixing. Results show the potential of laser-based manipulations to achieve precise control over the coherent spectrum in future x-ray FELs for new science[10, 11].

This material is based upon work supported by the U.S. Department of Energy, Office of Science, Office of Basic Energy Sciences, under Contract No. DE-AC02-76SF00515 and HEP.

The well-known echo effect is a highly nonlinear process that was originally described in 1950 by E. L. Hahn in the context of precessing nuclear spins[9]. Echoes have been observed in many areas of physics including cyclotron beams[12], plasma waves[13], photons[14], hadron colliders[15], molecular rotors in gas[16], and in classical mechanical systems[17]. Broadly described, echoes arise in a medium that is first excited by a perturbation that then damps completely due to dephasing. The inherent damping mechanism is non-dissipative, however, and the perturbations remain deeply encoded as highly filamentary structures in the phase space. Following an excitation by a second perturbation, the phase mixing is partially reversed as the system evolves, and the echo signal appears as a recoherence effect. This is the mechanism behind the proposed echo-enabled harmonic generation (EEHG) technique to produce fully coherent x-ray pulses in a free-electron laser (FEL)[7, 8]. EEHG exploits the fact that the fine phase-coherent echo structures have much higher frequency content than the original perturbations, so the temporal coherence of modulations imprinted by conventional lasers can be passed to shorter wavelengths, with the electrons serving as the harmonic up-conversion medium.

The EEHG concept is illustrated in the schematic of our experimental layout in Fig. 1. The E=120 MeV relativistic electron beam co-propagates with a laser pulse (λ_1=800 nm) in a magnetic undulator, U1 (see Methods). The resonant interaction imprints a sinusoidal energy modulation with amplitude ΔE_1 in the electron beam phase space (a). Linear longitudinal dispersion through the magnetic chicane C1, given by the transport matrix element $R_{56}^{(1)}$, allows electrons with different energies to move relative to one another as they traverse different path lengths. This phase-mixing transformation turns the sinusoidal modulation into a filamentary distribution with multiple energy bands (b). A second laser (λ_2=2400 nm) then produces an energy modulation (ΔE_2) in the finely striated beam in the U2 undulator (c). Finally the beam travels through the C2 chicane where a smaller dispersion $R_{56}^{(2)}$ brings the energy bands upright (d). Projected into the longitudinal space, the echo signal appears as a series of narrow current peaks (bunching) with separation $\lambda = \lambda_2/h$ (e), where h is a harmonic of the second laser which determines the character of the harmonic echo signal.

EEHG has been examined experimentally only recently at modest harmonic orders, starting with the 3rd and 4th harmonics[18, 19], the 7th harmonic[20], and most recently at the 15th harmonic[21] of IR lasers. These studies demonstrated that the EEHG harmonics are generated with small relative increases in the beam energy spread compared with high-gain harmonic-generation (HGHG) schemes[22–24], and also that the spectrum is much less sensitive to initial electron beam phase space distortions. However, to reach from UV seed lasers to the soft x-ray wavelengths where the most compelling scientific applications are found, harmonic numbers $h \geq$50 are required, which in turn requires exquisite preservation of the fine-scale phase-space memory.

Here we report on first results of EEHG experiments in the h=60 and h=75 harmonic regimes which also highlight the fine and unique control the echo mechanism provides over the coherent emission spectrum. Results suggest the possibility to precisely tailor the pulses in future x-ray FELs for new science applications[10, 11].

From EEHG theory, the optimal harmonic bunching b_h is tuned and scales according to the ratio of dispersions, $h \approx \lambda_2 R_{56}^{(1)}/\lambda_1 R_{56}^{(2)}$. Accordingly, the C1 chicane was set to $R_{56}^{(1)}$=12.5 mm, close to its peak value. In the first experiment, the dispersion of the second chicane was approximately $R_{56}^{(2)}$=600 μm to produce bunching near the 60th harmonic of the 2400 nm laser. The bunched beam was boosted to 192 MeV in a short linac (see Fig. 1) such that the $\lambda \approx$ 40 nm harmonic wavelengths were radiated at the 3rd harmonic of U3 emission spectrum (see Methods). Shown in Figure 2(a), the characteristic undulator radiation pattern is seen in the quadratic dependence of the wavelength on the vertical forward angle (see Methods), and the bright peaks are the coherent harmonic echo signals. The image is the average of over 200 consecutive shots, but is representative of typical single shots. The spectrum of each shot, taken from the vertical projection, is shown in Figure 2(b). Analysis of the spectral stability over all shots gives a 0.025 nm rms variation of the central wavelength of the 59th harmonic signal (0.063% relative). The observed bandwidth of each harmonic peak for each shot is equal to the measured 0.15 nm resolution of the EUV spectrometer (see Methods), but simulations indicate the true bandwidth to be 0.011 nm (FWHM). Simulations also show that the 1 ps lasers produce echo bunching in a 0.4 ps (FWHM) long portion of the $\sim$ 1 ps (FWHM) electron beam. The envelope of the average spectrum is shown in Fig. 2(c) (blue line), along with the spectrum of incoherent spontaneous radiation from the beam when both seed lasers are blocked (red line), which has a small bump at the 3rd undulator harmonic. Numerical simulations of the bunching indicate good agreement with the observed EEHG spectrum for ΔE_1=38 keV and ΔE_2=84 keV. These energy modulation amplitudes are consistent with those observed experimentally at the electron energy spectrometer. It is noted that, with laser 1 blocked no harmonic signals were observed, which confirms that the signal is due to the combination of modulations that produce an echo rather than HGHG bunching from a single laser.

To access the highest harmonics in our setup, dispersion in the second chicane was lowered towards its minimum value around $R_{56}^{(2)}$= 500 μm, and the EUV spectrometer moved to view the 75th harmonic regime at 32 nm. Coherent

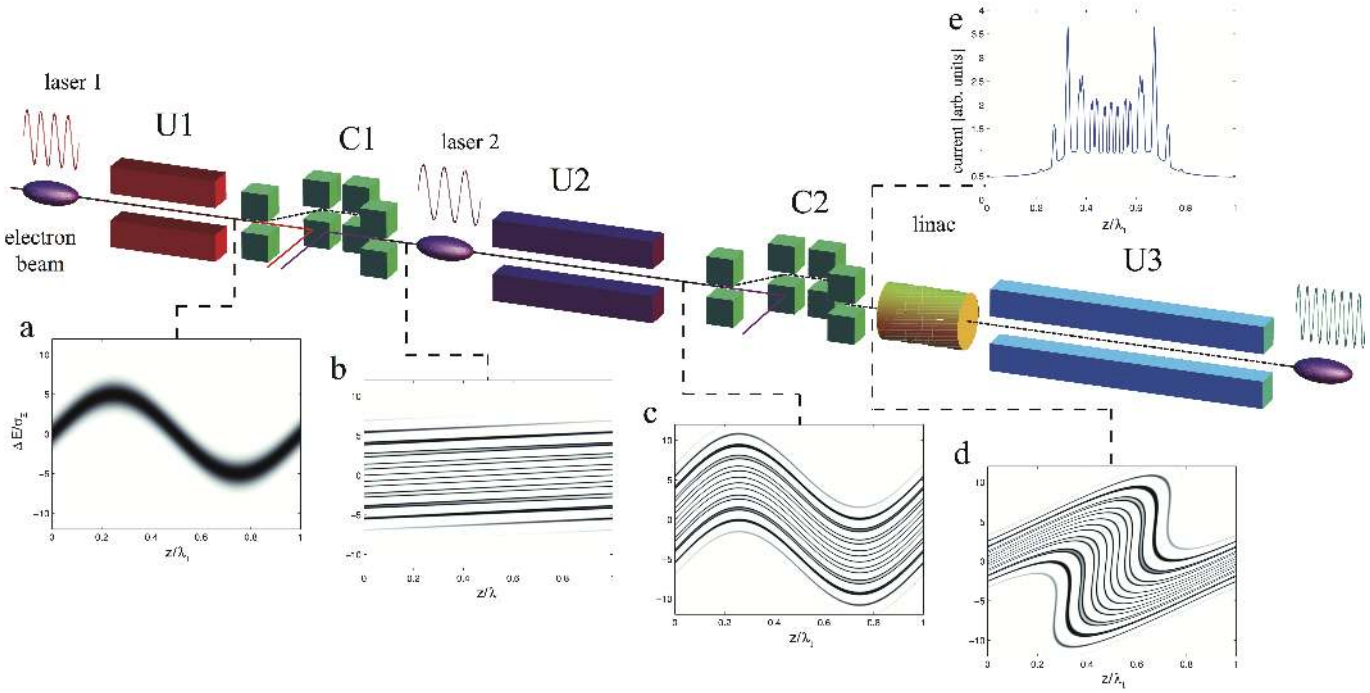

FIG. 1. Schematic layout of the echo beam line and evolution of the electron beam phase space after successive transformations. The final phase space distribution (d) has a series of vertical energy stripes that project to sharp peaks in the electron beam current distribution (e).

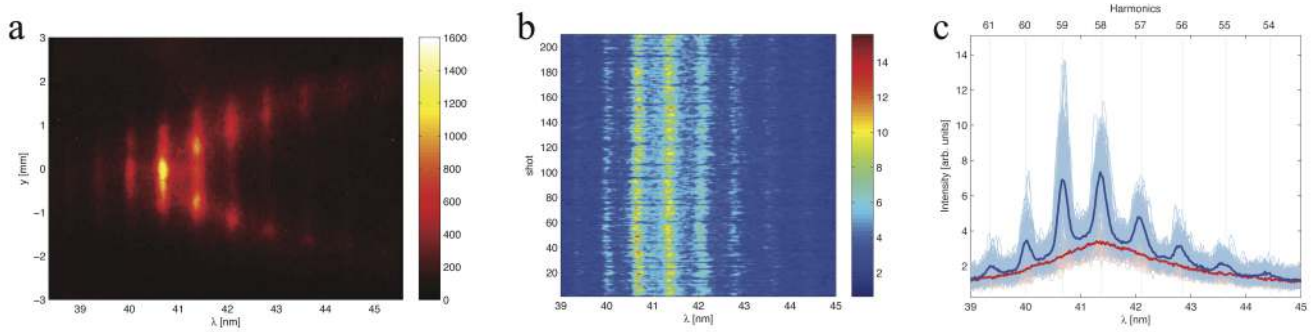

FIG. 2. Echo harmonics of the 2400 nm laser in the 60^{th} harmonic range. (a) Undulator emission. (b) Individual spectra over multiple consecutive shots. (c) Spectrum of the incoherent spontaneous radiation and the coherent echo signal.

emission in this case is peaked at the 4th harmonic resonance of U3, and thus is emitted slightly off-axis by the nature of even harmonic undulator emission. The measured spectra are shown in Fig. 3(a). With lasers on, the echo harmonics are clearly visible (blue lines), while with lasers off, only spontaneous radiation is observed (red). In Fig. 3 (b), the averaged spontaneous background (Fig. 3(a), dark red) is subtracted from the averaged echo spectrum (Fig. 3(a), dark blue), and results from numerical simulations for the bunching are compared with the measured coherent spectrum. Simulations indicate that energy modulations of ΔE_1=61 keV and ΔE_2=104 keV produce a harmonic spectrum that is strikingly similar to the data, both in the relative amplitude of the harmonics and in the variation of the envelope of harmonic peaks. Again, these values are consistent with experimental measurements. As was also the case with the experiments on the 60th harmonic, the observed shot-to-shot amplitude fluctuations were due primarily to charge fluctuations (as seen in the variation of the incoherent signal) and systematic intensity fluctuations in the second laser pulse (See Methods). With laser 1 blocked in this configuration, harmonics of the optimized HGHG signal were fully suppressed, which confirms the efficiency of the echo harmonic generation process.

It is important to note that the coherent signal at these wavelengths and at this beam energy is calculated to be strongly suppressed by longitudinal smearing effects of beam betatron motion in U3, due to the finite beam emittance

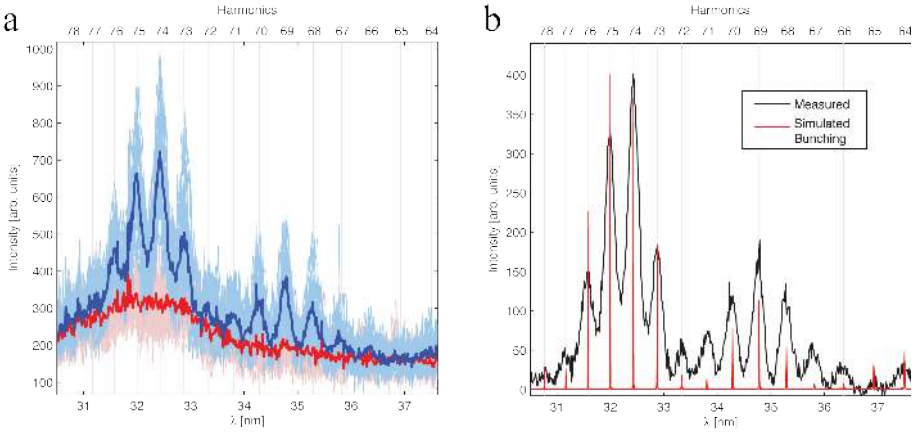

FIG. 3. Echo in the 75^{th} harmonic range. (a) Measured electron beam emission spectrum with echo lasers on (blue lines) and with lasers off (red lines). (b) Coherent signal with spontaneous emission spectrum subtracted (black) and the harmonic amplitudes of $|b_h^2|$ from numerical simulations (red).

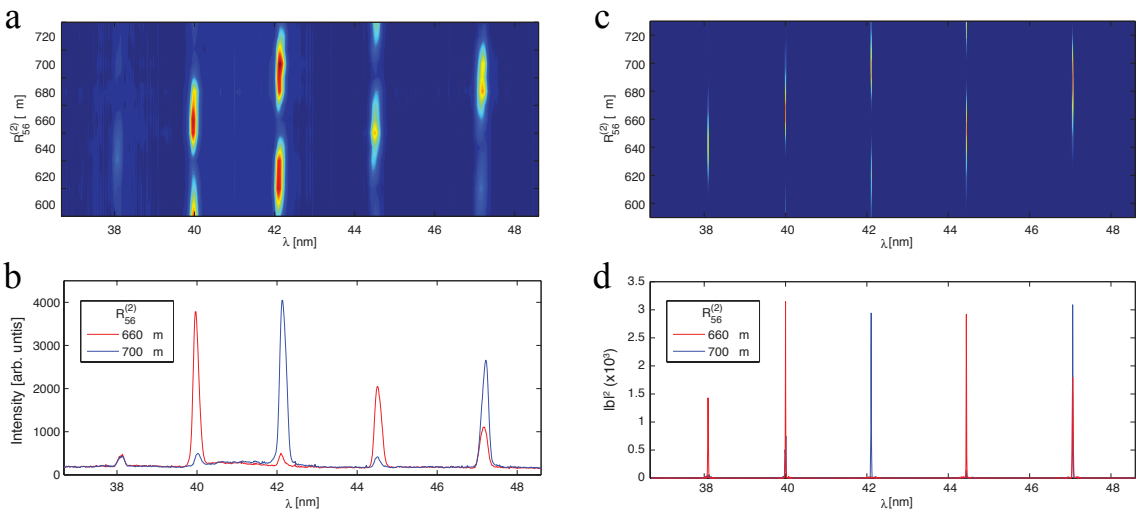

FIG. 4. Tuning harmonics with dispersion. (a) Individual echo harmonics of the λ_2=800 nm laser tuned as a function of the second dispersion $R_{56}^{(2)}$. (b) At certain dispersion values, specific harmonics are dominant while nearby harmonics are almost completely suppressed. (c) and (d) Matching results from numerical simulations for $|b_h|^2$, where the narrow bandwidth is resolved.

and the fixed U3 strong focusing channel. This likely accounts for the relative smallness of the coherent signal compared to the spontaneous background in both the 60th and 75th harmonic experiments. This effect becomes still stronger at shorter wavelengths, which precluded investigation of still higher harmonics in our setup, but is significantly reduced in optimized soft x-ray FELs with larger beta functions and higher energy beams (see Methods).

The variation of the harmonic envelope observed in Figure 3(b), where certain harmonics are suppressed (e.g., the 72nd) while nearby harmonics are enhanced (e.g., the 74th), is a newly observed and unique feature of the beam echo effect compared to HGHG. This effect is predicted from EEHG theory which indicates that the individual harmonics can be precisely tuned by the dispersion (see Methods). Results of a separate experiment to explore this harmonic tunability are presented in Fig. 4, where the measured spectrum in the neighborhood of the 20th harmonic from two 800 nm seed lasers are shown in (a) and (b). Here, ΔE_2 was held stable while the value of the $R_{56}^{(2)}$ was varied. Individual harmonics within the envelope are seen to be optimized at slightly different dispersion values. For instance, at $R_{56}^{(2)} = 660$ μm, bunching at 40 nm can be optimized while that at 42 nm can be suppressed; the 2 nm difference is more than two orders of magnitude smaller than the wavelength of the lasers used to create the fine structure. This precise control over the coherent beam distribution is also reproduced in simulations with ΔE_1=29 keV and ΔE_2=27 keV, as shown in Fig. 4(c) and (d).

Experiments thus show that the proposed beam echo effect can be used to produce ultra high harmonic bunching, and that it enables precise control via practical means over the fine scale bunching spectrum. Demonstration of EEHG at the 75th harmonic suggests that it may be straightforward to use this technique to seed the amplification of fully coherent and tunable soft x-rays in the water window (2-4 nm) above the GW level in a single stage from UV lasers in future FELs. Further, two-stage EEHG with the soft x-rays from the first stage seeding the second stage, might eventually allow extension to hard x-ray wavelengths.

ACKNOWLEDGEMENTS

The authors would like to thank D. McCormick, K. Jobe, I. Makasyuk, T. Beukers, C. Hudspeth, J. Cruz, V. Yakimenko, and the rest of the Test Facilities group for their support. We also thank M. Guehr for his guidance with the design and construction of the EUV spectrometer, and E. Johnson for the VISA undulator. This work was supported by the U.S. DOE Office of Basic Energy Sciences under award number 2012-SLAC-10032 using the SLAC NLCTA facility which is partly supported by U.S. DOE Office of High Energy Physics under Contract No. DE-AC02-76SF00515. The work of D.X. was supported by the Major State Basic Research Development Program of China (Grants No. 2015CB859700) and by the National Natural Science Foundation of China (Grants No. 11327902).

AUTHOR CONTRIBUTIONS

G.S. conceived the original EEHG theoretical concept, which was later developed further with D.X.. E.H., B.G., and M.D. carried out the experiments. B.G. and M.D. designed and built the EUV spectrometer. E.H. and B.G. performed the data analysis and performed simulations. D.X., C.H., and T.R. provided guidance on the experiments and on potential applications. E.H. and D.X. wrote the paper, with contributions from all other authors.

AUTHOR INFORMATION

The authors declare no competing financial interests.

CORRESPONDENCE

Correspondence and requests for materials should be addressed to E.H. (ehemsing@slac.stanford.edu) or D.X. (dxiang@sjtu.edu.cn).

[1] Maiman, T. H. Stimulated optical radiation in ruby. *Nature* 187, 493494 (1960).
[2] Schawlow, A. L. and Townes, C. H. Infrared and Optical Masers. *Phys. Rev.* 112, 1940 (1958).
[3] Franken, P. A., Hill, A. E., Peters, C. W. and Weinreich, G. Generation of Optical Harmonics. *Phys. Rev. Lett.* 7, 118 (1961).
[4] Emma, P. *et al.* First lasing and operation of an angstrom-wavelength free-electron laser. *Nature Photon.* 4, 641 (2010).
[5] Ishikawa, T. *et al.* A compact X-ray free-electron laser emitting in the sub-angstrom region. *Nature Photon.* 6, 540 (2012).
[6] McNeil, B. W. J. and Thompson, N. R. X-ray free-electron lasers. *Nature Photon.* 4, 8140 (2010).
[7] Stupakov, G. Using the Beam-Echo Effect for Generation of Short-Wavelength Radiation. *Phys. Rev. Lett.* 102, 074801 (2009).
[8] Xiang, D and Stupakov, G. Echo-enabled harmonic generation free electron laser. *Phys. Rev. ST Accel. Beams* 12, 030702 (2009).
[9] Hahn, E. L. Spin echoes. *Phys. Rev.* 80, 580 (1950).
[10] Hemsing, E., Stupakov, G., Xiang, D. and Zholents, A. Beam by design: Laser manipulation of electrons in modern accelerators. *Rev. Mod. Phys.* 86, 897 (2014).
[11] Schneider, J. R. Photon Science at Accelerator-Based Light Sources. *Reviews of Accelerator Science and Technology* 3, 13 (2010).
[12] Hill, R. M. and Kaplan, D. E. Cyclotron Resonance Echo. *Phys. Rev. Lett.* 14, 1062 (1965).
[13] Gould, R. W., O'Neil, T. M. and Malmberg, J. H. Plasma Wave Echo. *Phys. Rev. Lett.* 19, 219 (1967).
[14] Kurnit, N. A., Abella, I. D. and Hartmann, S. R. Observation of a Photon Echo. *Phys. Rev. Lett.* 13, 567 (1964).

[15] Spentzouris, L. K., Ostiguy, J.-F. and Colestock, P. L. Direct Measurement of Diffusion Rates in High Energy Synchrotrons Using Longitudinal Beam Echoes. *Phys. Rev. Lett.* 76, 620 (1996).
[16] Karras, G. *et al.* Orientation and Alignment Echoes. *Phys. Rev. Lett.* 114, 153601 (2015).
[17] Chebotayev, V. P. and Dubetsky, B. Ya. A classical model of the photon echo. *Appl. Phys. B* 31, 45 (1983).
[18] Xiang, D. *et al.* Demonstration of the Echo-Enabled Harmonic Generation Technique for Short-Wavelength Seeded Free Electron Lasers. *Phys. Rev. Lett.* 105, 114801 (2010).
[19] Zhao, Z. *et al.* First lasing of an echo-enabled harmonic generation free-electron laser. *Nature Photon.* 6, 360 (2012).
[20] Xiang, D. *et al.* Evidence of High Harmonics from Echo-Enabled Harmonic Generation for Seeding X-Ray Free Electron Lasers. *Phys. Rev. Lett.* 108, 024802 (2012).
[21] Hemsing, E. *et al.* Highly coherent vacuum ultraviolet radiation at the 15th harmonic with echo-enabled harmonic generation technique. *Phys. Rev. ST Accel. Beams* 17, 070702 (2014).
[22] Yu, L. H. Generation of intense uv radiation by subharmonically seeded single-pass free-electron lasers. *Phys. Rev. A* 44, 5178 (1991).
[23] Allaria. E. *et al.* Highly coherent and stable pulses from the FERMI seeded free-electron laser in the extreme ultraviolet. *Nature Photon.* 6, 699 (2012).
[24] Allaria. E. *et al.* Two-stage seeded soft-X-ray free-electron laser. *Nature Photon.* 7, 913 (2013).

METHODS

Experiments were conducted at the Next Linear Collider Test Accelerator (NLCTA) at SLAC National Accelerator Laboratory.

Electron beam.

The NLCTA electron beam is generated in a photocathode RF gun (RF frequency at 2.856 GHz) at 10 Hz repetition rate, and is boosted to E=120 MeV with two X-band linac structures (RF frequency at 11.424 GHz). The echo manipulations are performed at this energy. The electron beam charge is about 20 pC in the experiment, the FWHM bunch length is about 1 ps, the slice energy spread is about $\sigma_E \simeq$1-2 keV, and the projected normalized transverse emittance is approximately 1.7 μm. The beam current is kept low to avoid lasing in the undulator such that the undulator harmonics and off-axis emission angles provide a broadband diagnostic of the harmonic bunching spectrum. The measured rms energy variation about the final 190 MeV central energy is approximately 190 keV (0.1%). At this level, the $R_{56}^{(1)}$=12.5 mm dispersion in the first chicane leads to a 40 fs rms electron beam arrival time jitter in the downstream undulators.

Laser beam.

The two seed lasers originated from a single 800 nm ($\sim$ 1 ps FWHM) laser pulse that was sent through a beam splitter. One pulse seeded the U1 undulator at λ_1=800 nm, and the other pumped an optical parametric amplifier (OPA) to produce a λ_2=2400 nm pulse ($\sim$ 1 ps FWHM, $\leq$ 10 μJ) in the U2 undulator. The energy of the 2400 nm laser has considerable fluctuations due to the pointing stability and long transport of the 800 nm laser, which leads to relatively large shot-to-shot fluctuations of the echo signals in Fig. 2 and Fig. 3. The OPA can also be bypassed to allow modulating the beam in U2 with 800 nm seed laser. By using the two 800 nm lasers, the echo signals in Fig. 4 have much better energy stability.

Echo Beamline.

The echo beamline consists of three undulators (a series of magnets with alternating fields), two chicanes (a series of bending magnets that changes the electron's path length according to its energy) and one accelerator structure. The resonant wavelength of an undulator is $\lambda_r = \frac{\lambda_u}{2h_u\gamma^2}(1 + K^2/2 + \theta^2\gamma^2)$, where λ_u is the undulator period, K is the normalized undulator parameter, h_u is the undulator harmonic, γmc^2 is the beam energy in the undulator, and θ is the forward emission angle. U1 has 10 periods, each with length of λ_u=3.3 cm and an undulator parameter of K=1.82. The beam then transits the C1 chicane, and then co-propagates with the second laser pulse (λ_2=2400 nm if from the OPA, λ_2=800 nm if the OPA is bypassed) inside the U2 undulator (10 periods with a period length of 5.5 cm and

K=2.76). The tuning of U2 is such that the 2400 nm laser pulse is resonant with the 120 MeV ($\gamma = 235$) beam at the 1st harmonic (h_u=1) of the undulator, and the 800 nm pulse is resonant with the 3rd harmonic. After passage through the C2 chicane, the beam is accelerated up to a maximum of 192 MeV by a 1.05 m long x-band linac. Radiation is produced by the beam inside the U3 undulator (110 periods with a period length of 1.8 cm (L = 198 cm total length) and K=1.26). The U3 is a 2 m section of the VISA-II Halbach-type pure-permanent magnet undulator with 8 distributed strong focusing FODO cells, each of 24.75 cm length [1]. At E=190 MeV (γ=372), the on-axis resonance of our U3 undulator is 117 nm at the $h_u = 1$ fundamental. Four intra-undulator retractable beam profile screens imaged by CCD cameras allow electron beam orbit and beta-matching correction with external steering magnets and upstream quadrupoles, respectively.

Each four-dipole chicane is remotely adjustable but has a minimum dispersion to allow the electron beam to pass cleanly by the laser injection/rejection mirror assembly, which is between the second and third dipoles. This sets the geometric minimum R_{56} to about 500 μm to avoid beam scraping, but there is a known uncertainty of 100 μm in the recorded dispersion at these small values. Each chicane also has two magnetic quadrupoles for horizontal dispersion correction; one positioned halfway between the first and second dipole, and one halfway between the third and fourth dipole.

Laser and electron beam overlap.

Effective interaction between the lasers and electron beam is achieved when electron and laser beam overlap both spatially and temporally in the modulators. The spatial overlap between the 800 nm laser and the electron beam is achieved by steering the laser to the same position as the beam on the screens upstream and downstream of the undulators. The temporal overlap is achieved with two steps. First, an optical transition radiation screen downstream of each undulator is used to reflect out the laser and undulator radiation which is detected by a fast photodiode. By referencing the signals to an external trigger, the laser and electron beam can be synchronized to within approximately 30 ps. More precise timing is then done by using a scanning delay stage and measuring coherent transition radiation from the electron beam downstream of C1. The second laser at 2400 nm is made to overlap with the beam in U2 a similar way. Unattenuated, the 2400 nm idler pulse profile can be seen with the CCD beam profile cameras for transverse overlap with the electrons. A bandpass filter centered at 2400 nm is used in the experiment to ensure that the beam is only modulated by the 2400 nm laser in U2, and not the 1200 nm signal pulse from the OPA.

EUV Spectrometer.

Coherent EUV radiation emitted by the beam in U3 is measured with a high resolution, custom-built, ultra high vacuum spectrometer with sensitivity in the 11-62 nm wavelength range [2]. Radiation is first reflected off an insertable gold coated mirror at 15° incidence ∼0.5 m downstream of U3, and sent through an extraction port off the beam line. The light then passes through a slit with independently adjustable blades and then strikes a Hitachi 001-0640 aberration-corrected concave grating with 1200 G/mm at an incidence angle of 4.7°. The blaze angle is 3.7°, and the grating images the slit at a flat field focus 469 mm from the center. The combined assembly allows 60-80% efficiency over the wavelengths of interest. This grating is fixed-mounted in a custom high-vacuum chamber connected to a large bellows that allows the light to travel to the 40 mm MicroChannel Plate (MCP) detector (Model BOS-40, Beam Imaging Solutions, ≤2 kV power supply). Behind the MCP is a P-43 phosphor screen, powered by a ≤5 kV power supply, which is then directly imaged with a CCD camera. The MCP/phosphor/camera assembly is mounted to a linear motion stage that allows 120 mm of translation parallel to the grating focal plane to capture the full wavelength range, including the zeroth order. Calibration of the spectrometer is done using the known grating equations in combination with the harmonic radiation spectrum from the undulator and the echo harmonics from the 800nm/2400nm and 800nm/800nm laser seeding configurations. The spectrometer can be set to capture different harmonic emission of the U3 undulator.

Simulations.

Numerical simulations use the measured realistic beam distributions, laser energy modulations and chicane dispersions. Electrons are tracked through the echo beamline and the final beam distribution is used to calculate the bunching at various wavelengths. The dispersion in C1 is taken as $R_{56}^{(1)}$=12.5 mm and the electron beam length is

0.43 ps rms for all simulations. For the Echo 75 simulations in Fig. 3(b), $R_{56}^{(2)}$=484 μm (in good agreement with the measured value considering the uncertainty of the dispersion near the minimal value), ΔE_1=61 keV, and ΔE_2=104 keV. With a seed laser pulse length of 1 ps FWHM, simulations indicate that the coherent bunching extends over 0.4 ps of the electron beam, and that the FWHM bandwidth of $|b_h|^2$ is 0.007 nm at 32 nm. In Fig. 4, the parameters used in the simulation are ΔE_1=29 keV, ΔE_2=27 keV, and $R_{56}^{(2)}$=590-730 μm.

Bunching factor.

From EEHG theory, the bunching amplitude at the bunching frequency $\omega_{n,m} = n\omega_1 + m\omega_2$ is

$$b_h = e^{-\xi^2/2} J_n\left(-\xi \Delta E_1/\sigma_E\right) J_m\left[-\omega_{n,m}\Delta E_2 R_{56}^{(2)}/cE\right], \tag{1}$$

where $\omega_{1,2} = 2\pi c/\lambda_{1,2}$ are the seed laser frequencies, $\xi = (\sigma_E/cE)(n\omega_1 R_{56}^{(1)} + \omega_{n,m} R_{56}^{(2)})$, and $J_{n,m}$ are Bessel functions. In practice, the modulations and dispersions are tuned so that b_h is maximized at the desired echo harmonic of the second laser $h = \omega_{n,m}/\omega_2 = m + n(\omega_1/\omega_2)$ for a given n and m, where m is typically large, and $n < 0$ with $|n|$ small. Optimized echo harmonics are given in general approximately by the ratio $h \approx -n\lambda_2 R_{56}^{(1)}/\lambda_1 R_{56}^{(2)}$. In all of our experiments, the tune was such that $n = -1$.

Smearing of bunching.

The beam betatron motion in U3 results in longitudinal smearing effects that reduce the bunching factor at high harmonic frequencies. This is due to the fact that particles with larger betatron amplitudes have longer path lengths. The longitudinal smearing effect is estimated as $\Delta z = \sqrt{2}\epsilon_n L/\gamma\langle\beta\rangle \approx$5 nm which is comparable to $\lambda/2\pi$, where L=2 m is the length of the undulator U3, $\epsilon_n \approx$0.5 mm-mrad is the (assumed) electron beam slice transverse emittance, $\langle\beta\rangle$=65 cm is the average beta function in U3, and λ is the wavelength of the harmonic radiation. The beta function in the undulator is fixed by the permanent magnetic focusing at the 190 MeV beam energy, so the beta function of the beam cannot be increased to mitigate this effect without mismatching the beam. In the absence of this smearing effect, simulations indicate a bunching factor of several percent, depending on the harmonic tune. Given that the effective bunching due to noise is $b_{SN} \sim 1/\sqrt{N_s} \sim 4 \times 10^{-4}$ (where N_s is the number of electrons in a slippage length $L\lambda_r/\lambda_u$), this would result in an increase of the coherent emission by about four orders of magnitude above the incoherent background. Similarly, for optimized FELs operating in the water window, the few percent echo bunching factor is also about two orders of magnitude higher than shot noise bunching, which enables the production of fully coherent radiation.

[1] Carr, R. *et al*, Visible-infrared self-amplified spontaneous emission amplifier free electron laser undulator. *Phys. Rev. ST Accel. Beams* 4, 122402 (2001).

[2] Garcia, B., Dunning, M. P., Hast, C., Hemsing, E. and Raubenheimer, T. O. Facility upgrades for the high harmonic echo program at SLAC's NLCTA. Proceedings of FEL 2015, Daejeon, Korea.